

Pomeron in diffractive processes $\gamma^*(Q^2)p \rightarrow \rho^0 p$ and $\gamma^*(Q^2)p \rightarrow \gamma^*(Q^2)p$ at large Q^2 : the onset of pQCD

V. V. Anisovich, L. G. Dakhno, D. I. Melikhov, V. A. Nikonov, and M. G. Ryskin
St. Petersburg Nuclear Physics Institute, Gatchina, 188350, Russia
(August 15, 2018)

We study the reactions $\gamma^*(Q^2)p \rightarrow \rho^0 p$ and $\gamma^*(Q^2)p \rightarrow \gamma^*(Q^2)p$ at large Q^2 and W^2/Q^2 and small momentum transfer, κ_\perp^2 , to the nucleon where the pomeron exchange dominates. At large Q^2 the virtual photon selects a hard $q\bar{q}$ pair, thus selecting the hard pomeron component (the BFKL pomeron). The amplitudes for both transverse and longitudinal polarizations of the initial photon and outgoing ρ -meson (photon) are calculated in the framework of the BFKL pomeron exchange. Our calculations show that one cannot expect the early onset of the pure perturbative regime in the discussed diffractive processes: the small interquark distances, $\rho_{q\bar{q}} < 0.2$ fm, start to dominate not earlier than at $Q^2 \simeq 100$ GeV², $W^2/Q^2 \simeq 10^7$ in $\gamma^*(Q^2)p \rightarrow \rho^0 p$ and $Q^2 \simeq 50$ GeV², $W^2/Q^2 \simeq 10^6$ in $\gamma^*(Q^2)p \rightarrow \gamma^*(Q^2)p$.

I. INTRODUCTION

In the present paper we continue a study of the onset of the perturbative QCD regime in the processes initiated by virtual photon $\gamma^*(Q^2)$ along the lines of [1,2]. One may address two types of hard processes which allow one to study the transition regime from the Strong-QCD physics to the perturbative QCD physics of hard processes at accessible energies: these are (i) hard hadronic form factors [3,4], and (ii) pomeron-dominated reactions [5,6].

An important problem which arises in the quantitative description of hard processes is a numerical determination of the scale at which the perturbative regime starts to dominate the amplitudes of interest. Much attention to this subject has been paid in connection with the elastic form factors [7,8]. In particular, the authors of [7] advocated the viewpoint of an early applicability of pQCD at considerably low Q^2 , whereas in [8] the arguments in favour of the late onset of the perturbative regime, at very large $Q^2 \simeq 50$ GeV², were given. A quantitative study of [1] confirmed the arguments of ref. [8] and showed that even at Q^2 as large as 20 GeV² the form factor is still dominated by the soft non-perturbative region of the $q\bar{q}$ kinematical configurations. In [1,2] the elastic pion and transition form factors were studied at $0 \leq Q^2 \leq 100$ GeV² within an approach where both the truly non-perturbative and perturbative contributions have been taken into account. Namely, the form factor has been represented as a sum of the triangle diagram (direct convolution of soft wave functions) and diagrams with the one-gluon exchanges (the convolution of hard one-gluon exchange kernel with soft wave functions). The analysis of form factors in the region of small $Q^2 \sim 0-1$ GeV² allowed us to reconstruct phenomenological soft wave functions of pseudoscalar mesons and soft photon. It was found that the diagrams with the one-gluon exchange (the terms of the order of α_s) started to dominate the form factor only at $Q^2 > 50$ GeV², whereas at smaller Q^2 the contribution of non-perturbative triangle diagram was substantial.

In this work we address diffractive production by the hard photon, namely the reactions $\gamma^*(Q^2)p \rightarrow \rho^0 p$ and $\gamma^*(Q^2)p \rightarrow \gamma^*(Q^2)p$.

One would have in mind the following physical picture of such processes at asymptotically large Q^2 : the virtual photon produces $q\bar{q}$ pair at small distances (see Fig. 1), then the quarks convert into vector meson (or outgoing photon) with the t -channel emission of gluons: the gluons at the top of the ladder are at relatively small distances and thus a hard component of the pomeron (i.e. the BFKL pomeron [5]) is selected. The lower part of the gluon ladder is attached to the nucleon at small momentum transfer, and thus the region of small transverse momenta is selected at the bottom of the ladder. Hence the most realistic is the following scenario of the whole reaction: typical virtualities in the gluon ladder change from hard values selected by the virtual photon in the hard quark-loop at the top of the ladder to the soft values at the bottom, and thus the whole t -channel behavior is determined by the complicated object which is a superposition of the hard and the soft pomerons. The details of the partition of the whole t -channel amplitude into the hard and soft components depend on the values of Q^2 and specific details of the selection of the hard component of the Pomeron by the quark loop. That is why a detailed consideration of the hard upper quark-antiquark subprocess based on realistic wave functions of the initial photon and the outgoing vector meson is crucial for the understanding of the mechanism of the reaction at large but finite Q^2 .

Notice that the interest in better understanding of the diffractive production mechanism is also motivated by the experimental results. Experimentally a rather strong change of the W -dependence of the cross section of the reactions initiated by the photon in different regions of the photon virtuality has been observed: Namely, the W dependence of the cross section of the photoproduction ($Q^2 = 0$) in the region $W \sim 10 - 200$ GeV² is rather flat, similar to that

in hadronic processes like $\pi p \rightarrow \pi p$. However, the reaction $\gamma^*(Q^2)p \rightarrow Vp$ at $Q^2 \sim 10 - 20 \text{ GeV}^2$ demonstrates an increase of the cross section with W as $W^{2\Delta}$ where $\Delta \approx 0.3$. An attractive possibility one might think of is to refer this growth to the change of the pomeron regime from the Strong-QCD one at small Q^2 to the BFKL one at large Q^2 . However, for better understanding of this phenomenon one needs a more detailed quantitative analysis of the different ingredients of a complicated amplitude of the diffractive production.

In this paper we concentrate on the quark block with a coupled photon, $\gamma^*(Q^2)$, which is responsible for a selection of the region of small separations and thus of the hard pomeron component. The quark block is determined by the convolution of photon wave functions (the reaction $\gamma^*(Q^2)p \rightarrow \gamma^*(Q^2)p$) or convolution of the photon and ρ -meson wave functions (the reaction $\gamma^*(Q^2)p \rightarrow \rho^0 p$).

The light-cone wave function of photon was found in ref. [2] on the basis of experimental data for the transition form factor $\gamma\gamma^*(Q^2) \rightarrow \pi^0$ at $0 \leq Q^2 \leq 25 \text{ GeV}^2$ [9]; this wave function was successfully applied for the description of data on $\gamma\gamma^*(Q^2) \rightarrow \eta$ and $\gamma\gamma^*(Q^2) \rightarrow \eta'$ [9,10]. The analysis of the transition form factors has been performed in terms of the double spectral representation over $q\bar{q}$ invariant mass squared, $M_{q\bar{q}}^2 = (m^2 + k_\perp^2) / (x(1-x))$ where k_\perp^2 and x are the components of the light-cone quark momenta, and m is the constituent quark mass. The photon wave function is represented as a sum of two components which correspond to a direct production of the $q\bar{q}$ pair with a point-like vertex $\gamma^* \rightarrow q\bar{q}$ at large $M_{q\bar{q}}$, and to the production in the low- $M_{q\bar{q}}$ region where the vertex has a nontrivial structure due to the soft $q\bar{q}$ interaction. The soft $q\bar{q}$ interaction yields an enhancement of the contribution of low-masses and respectively large distances in the quark loop.

With the light-cone wave function of the photon at hand we can calculate longitudinal and transverse polarization cross sections $\gamma_L^*(Q^2)p \rightarrow \gamma_L^*(Q^2)p$ and $\gamma_T^*(Q^2)p \rightarrow \gamma_T^*(Q^2)p$.

The onset of pQCD regime depends on the selection of small interquark separations in a quark loop with Q^2 . So, it is important to test which fraction of the cross-section as a function of Q^2 is actually gained at small transverse separations. Therefore, in parallel with calculating the $\gamma_{L,T}^*(Q^2)p \rightarrow \gamma_{L,T}^*(Q^2)p$ cross section which includes contribution of all transverse separations in the quark-loop coupled to the BFKL pomeron, we also calculate the part of this cross section which is actually gained at small $q\bar{q}$ distances $\rho_{q\bar{q}} < 0.2 \text{ fm}$. Strictly speaking, only this part of the cross section probes the BFKL pomeron, whereas the cross section where the quarks in the loop are at large distances should be rather coupled to the soft strong-QCD pomeron.

The results of our analysis show that in the region $Q^2 \sim 5 - 50 \text{ GeV}^2$ the $\gamma^*(Q^2)p \rightarrow \gamma^*(Q^2)p$ cross section is dominated by the domain of large transverse quark separations. The small quark separations in the loop start to dominate the cross section only at $Q^2 \geq 50 \text{ GeV}^2$ and $W^2/Q^2 \geq 10^6$.

This means that $\gamma^*(Q^2)$ selects small distances in the $\gamma^*\gamma^*$ -pomeron vertex approximately at the same values of Q^2 as it was in the pion elastic and transition $\gamma \rightarrow \pi, \eta, \eta'$ form factors.

The ρ -meson wave function necessary for the description of the reaction $\gamma^*(Q^2)p \rightarrow \rho^0 p$ is not known promptly, so we have to use some assumptions concerning the details of its behavior. The low- $M_{q\bar{q}}$ component of the ρ -meson wave function is supposed to be approximately the same as for a pion. The latter was found in [1] from fitting the data for pion form factor at $0 \leq Q^2 \leq 10 \text{ GeV}^2$ [11]. Moreover, the ρ -meson low- $M_{q\bar{q}}$ wave function should be close to photon's one due to the vector-meson dominance.

The high-mass component of the ρ -meson wave function needs a special discussion: for its calculation, we cannot apply exactly the same procedure as for the pion form factor. In the analysis of pion form factor [1], all the corrections of the order of α_s were taken into account. To this end, the wave function of the pion was splitted into soft and hard components, Ψ^S and Ψ^H , in the following way

$$\Psi^S \text{ is dominant at } M_{q\bar{q}} < M_0, \quad \Psi^H \text{ is dominant at } M_{q\bar{q}} > M_0. \quad (1)$$

The parameter M_0 , which separates the soft and hard regions, is expected to be of the order of several GeV; in [1] the value $M_0 = 3 \text{ GeV}$ was chosen: this corresponds to $|\vec{k}_0|^{-1} = (M_0^2/4 - m^2)^{-\frac{1}{2}} \simeq 0.15 \text{ fm}$ at $m \simeq 350 \text{ MeV}$. The separation of soft and hard wave functions was done in a simplest way using the step-function:

$$\Psi_\pi = \Psi^S \theta(M_0 - M_{q\bar{q}}) + \Psi^H \theta(M_{q\bar{q}} - M_0). \quad (2)$$

The hard component Ψ^H is a convolution of the soft wave function Ψ^S and hard gluon exchange kernel V^{α_s} :

$$\Psi^H = V^{\alpha_s} \otimes \Psi^S, \quad (3)$$

The splitting of the wave function into the soft and hard components yields the following expansion of the form factor over α_s

$$F = F^{SS} + 2F^{SH} + O(\alpha_s^2) \quad (4)$$

where F^{SS} is the soft form factor, and F^{SH} is the soft-hard contribution of the order $O(\alpha_s)$ which is determined by the diagram with the hard gluon exchange, Eq. (3). In this way, including the Sudakov form factor and renormalizing the quark mass, we have taken into account all the terms of the order $O(\alpha_s)$ in Eq. (4).

A proper consideration of all the α_s terms in the reaction $\gamma^*(Q^2)p \rightarrow \rho^p$ is a much more complicated task since such terms appear not only as corrections to the ρ -meson vertex but also as the next-to-leading order corrections to the BFKL-pomeron [12] and pomeron- $q\bar{q}$ vertex. Such kind of analysis lies beyond the scope of our present work. At the same time, the calculation of the $\gamma^*(Q^2)p \rightarrow \rho^0 p$ amplitude with taking into account only a part of the α_s corrections is not consistent.

In this situation, it seems reasonable to consider two extreme cases of the behavior of the $\rho \rightarrow q\bar{q}$ vertex at large $M_{q\bar{q}}^2$: first, $G_\rho(M_{q\bar{q}}^2) \simeq M_{q\bar{q}}^{-2}$ and second $G_\rho(M_{q\bar{q}}^2) = \text{const} \sim O(\alpha_s)$. In both considered cases the dominance of the region of small interquark separations $\rho_{q\bar{q}} < 0.2$ fm was not observed at least at $Q^2 \leq 50$ GeV² and $W^2/Q^2 \geq 10^6$.

The paper is organized as follows:

In Section II we discuss the kinematics of the reaction, the Lorentz structure of the amplitudes and some principal points of the spectral representations. Section III presents a detailed calculation of the amplitudes in the framework of the spectral representations over the invariant $q\bar{q}$ -mass. The numerical results are discussed in Section IV. In Conclusion we summarize the main results and present our viewpoint on the Strong-QCD pomeron and the electoproduction of vector mesons at $Q^2 < 100$ GeV².

II. KINEMATICS OF THE REACTIONS AND THE LORENTZ STRUCTURE OF THE AMPLITUDES

In this Section we describe the kinematics of the reaction and outline the principle points in the dispersive representation of the amplitude. Further technical details and final analytical expressions are given in the next Section.

We use the following notation for the four-vector of the particles involved: the initial virtual photon four-momentum q , the final virtual photon (or vector meson) four-momentum q' , the target nucleon momentum p_N , and the outgoing nucleon momentum p'_N . The following momentum conservations are imposed:

$$q' = q - \kappa, \quad p'_N = p_N + \kappa, \quad q + p_N = q' + p'_N. \quad (5)$$

The reaction is characterized by three independent kinematical variables $Q^2 = -q^2$, $W = (p_N q)/m_N$, and κ^2 , since $p_N^2 = p'^2_N = m_N^2$ and $q'^2 = \mu_V^2$ for $\gamma^*(Q^2)p \rightarrow Vp$ or $q'^2 = -Q^2$ for $\gamma^*(Q^2)p \rightarrow \gamma^*(Q^2)p$.

We are interested in the kinematics when

$$Q^2 \text{ is large, } W^2/Q^2 \gg 1, \quad \text{and } \kappa^2 \rightarrow 0. \quad (6)$$

It is convenient to describe the process in the reference frame where the target nucleon is at rest $p_N = (m_N, 0, 0)$ and photon fastly moving along the longitudinal axis z . The kinematical conditions (6) then imply that $q_z \rightarrow \infty$ and omitting the $1/q_z^2$ terms we come to the following expressions for the momentum and polarization vectors of the incoming photon

$$q = (q_z - \frac{Q^2}{2q_z}, 0, q_z), \quad \epsilon_L^{(\gamma)}(Q^2) = \frac{1}{iQ}(q_z, 0, q_z - \frac{Q^2}{2q_z}), \quad \epsilon_T^{(\gamma)}(Q^2) = (0, \vec{e}_\perp^{(\gamma)}, 0). \quad (7)$$

For the outgoing vector meson in the reaction $\gamma^*(Q^2)p \rightarrow Vp$, one has

$$q' = (q'_z + \frac{\mu_\perp^2}{2q'_z}, -\vec{\kappa}_\perp, q'_z), \quad \epsilon_L^{(V)}(\mu^2) = \frac{1}{\mu_\perp}(q'_z, 0, q'_z + \frac{\mu_\perp^2}{2q'_z}), \quad \epsilon_T^{(V)} = (0, \vec{e}_\perp^{(V)}, 0). \quad (8)$$

where $\mu_\perp^2 = \mu^2 + \kappa_\perp^2$ and $\vec{e}_\perp^{(V)} \vec{\kappa}_\perp = 0$. In the limit $\kappa_\perp^2/m_N \rightarrow 0$, the momenta q'_z and κ are equal to

$$q'_z = q_z - \frac{\mu_\perp^2 + Q^2}{2q_z}, \quad \kappa = q - q' = (0, \vec{\kappa}_\perp, \frac{\mu_\perp^2 + Q^2}{2q_z}). \quad (9)$$

Similar expressions determine the momentum and polarization vectors of the outgoing photon in the reaction $\gamma^*(Q^2)p \rightarrow \gamma^*(Q^2)p$: one needs to substitute $\mu_V^2 \rightarrow -Q^2$. Because of that we present below the formulas for the vector meson production only.

Instead of the nucleon momentum p_N , it is convenient to characterize the reaction under the kinematical conditions (6) by the vector

$$n = \frac{1}{q_0 + q_z}(1, 0, -1). \quad (10)$$

The vectors q and n determine the plane for longitudinal polarization, whereas the transverse plane is determined by transverse components of the vector κ . Notice that $n^2 = 0$ and $qn = -1$.

The amplitude of the reaction can be written in the form

$$A = \epsilon_\mu^{(\gamma)} A_{\mu\nu}(q, q', n) \epsilon_\nu^{(V)}, \quad (11)$$

where, due to the gauge invariance, the tensor $A_{\mu\nu}$ satisfies the relations $q^\mu A_{\mu\nu}(q, q', n) = q'^\nu A_{\mu\nu}(q, q', n) = 0$, thus having the following Lorentz structure:

$$\begin{aligned} A_{\mu\nu}(q, q', n) = & -(g_{\mu\nu} - \frac{n_\mu q_\nu}{nq} - \frac{q'_\mu n_\nu}{nq'} + \frac{qq'}{(nq)(nq')} n_\mu n_\nu) A_T(q^2, q'^2, nq, \kappa^2) \\ & + (q^2 n_\mu - nq \cdot q_\mu)(q'^2 n_\nu - nq' \cdot q'_\nu) A_L(q^2, q'^2, nq, \kappa^2) + O(\kappa_\mu, \kappa_\nu), \end{aligned} \quad (12)$$

and $O(\kappa_\mu, \kappa_\nu)$ stands for other possible tensor structures transversal with respect to q_μ and q'_ν and proportional to κ . In the limit $\kappa \rightarrow 0$ they do not contribute to the cross section and are omitted.

The cross sections are connected with the introduced amplitudes as follows:

$$\frac{d\sigma(\gamma_T^*(Q^2)p \rightarrow V_T p)}{d(-\kappa^2)} = |A_T|^2; \quad \frac{d\sigma(\gamma_L^*(Q^2)p \rightarrow V_L p)}{d(-\kappa^2)} = Q^2 \mu_V^2 |A_L|^2, \quad (13)$$

where we have omitted the terms proportional to κ^2 . The invariant amplitudes $A_{L,T}$ are connected with $A_{\mu\nu}$ through the following relations:

$$A_T = -\epsilon_{T\mu}^{(\gamma)}(Q^2) A_{\mu\nu}(q, q', n) \epsilon_{T\nu}^{(V)}(\mu_V^2), \quad A_L = \frac{1}{i\mu_V Q} \epsilon_{L\mu}^{(\gamma)}(Q^2) A_{\mu\nu}(q, q', n) \epsilon_{L\nu}^{(V)}(\mu_V^2). \quad (14)$$

One can write the spectral representations for the invariant amplitudes $A_{L,T}$ as follows:

$$A_{L,T}(q^2, q'^2) = \int \frac{dM_{q\bar{q}}^2 dM_{q\bar{q}}'^2}{\pi^2} \frac{\text{disc}_{M_{q\bar{q}}^2} \text{disc}_{M_{q\bar{q}}'^2} A_{L,T}(M_{q\bar{q}}^2, M_{q\bar{q}}'^2)}{(M_{q\bar{q}}^2 - q^2)(M_{q\bar{q}}'^2 - q'^2)}. \quad (15)$$

In order to obtain the double spectral densities $\text{disc}_{M_{q\bar{q}}^2} \text{disc}_{M_{q\bar{q}}'^2} A_{L,T}(M_{q\bar{q}}^2, M_{q\bar{q}}'^2)$ we must consider the process with the off-shell incoming and outgoing particles. Namely, we have the following off-shell momenta

$$q' \rightarrow P', \quad q \rightarrow P, \quad (16)$$

where

$$P^2 = M_{q\bar{q}}^2, \quad P'^2 = M_{q\bar{q}}'^2, \quad (P' - P)^2 = \kappa^2, \quad (17)$$

but

$$P - P' \neq \kappa, \quad (18)$$

if we take into account the terms of the order of $1/q_z$ and omit $O(1/q_z^2)$ -terms. The components of the off-shell incoming P and outgoing P' momenta can be chosen as follows:

$$P = (q_z + \frac{M_{q\bar{q}}^2}{2q_z}, 0, q_z), \quad P' = (q_z + \frac{M_{q\bar{q}}'^2 + \kappa_\perp^2}{2q_z}, -\vec{\kappa}_\perp, q_z). \quad (19)$$

The off-shell amplitude $A_{\mu\nu}(P, P', n)$ has a similar decomposition in terms of P, P', n as has the amplitude $A_{\mu\nu}(q, q', n)$ of Eq. (12) in terms of q, q', n .

Let us introduce the polarization vectors of the off-shell vector particles. The corresponding longitudinal polarization vectors are

$$\epsilon_L^{(P)}(M_{q\bar{q}}^2) = \frac{1}{\sqrt{M_{q\bar{q}}^2}}(q_z, 0, q_z + \frac{M_{q\bar{q}}^2}{2q_z}), \quad \epsilon_L^{(P')} (M_{q\bar{q}}'^2) = \frac{1}{\sqrt{M_{q\bar{q}}'^2 + \kappa_\perp^2}}(q_z, 0, q_z + \frac{M_{q\bar{q}}'^2 + \kappa_\perp^2}{2q_z}). \quad (20)$$

The transverse polarization vectors of the off-shell particles are equal to the transverse polarization vectors of the incoming and outgoing particles.

The amplitudes $A_{L,T}$ are connected with $A_{\mu\nu}$ as follows:

$$A_T = -\epsilon_{T\mu}^{(P)} A_{\mu\nu}(P, P', n) \epsilon_{T\nu}^{(P')}, \quad A_L = \frac{1}{\sqrt{M_{q\bar{q}}^2 M'_{q\bar{q}}{}^2}} \epsilon_{L\mu}^{(P)} A_{\mu\nu}(P, P', n) \epsilon_{L\nu}^{(P')}, \quad (21)$$

where the factor $\sqrt{M_{q\bar{q}}^2 M'_{q\bar{q}}{}^2}$ is just the following expression:

$$\epsilon_{L\mu}^{(P)} (P^2 n_\mu - n P \cdot P_\mu) (P'^2 n_\nu - n P' \cdot P'_\nu) \epsilon_{L\nu}^{(P')} = \frac{\sqrt{M_{q\bar{q}}^2 M'_{q\bar{q}}{}^2}}{\sqrt{M_{q\bar{q}}^2 + \kappa_\perp^2}} \simeq \sqrt{M_{q\bar{q}}^2 M'_{q\bar{q}}{}^2}. \quad (22)$$

Hence,

$$\begin{aligned} \text{disc}_{M_{q\bar{q}}^2} \text{disc}_{M'_{q\bar{q}}{}^2} A_T &= \text{disc}_{M_{q\bar{q}}^2} \text{disc}_{M'_{q\bar{q}}{}^2} \epsilon_{T\mu}^{(P)} A_{\mu\nu}(P, P', n) \epsilon_{T\nu}^{(P')}, \\ \text{disc}_{M_{q\bar{q}}^2} \text{disc}_{M'_{q\bar{q}}{}^2} A_L &= \text{disc}_{M_{q\bar{q}}^2} \text{disc}_{M'_{q\bar{q}}{}^2} \epsilon_{L\mu}^{(P)} A_{\mu\nu}(P, P', n) \epsilon_{L\nu}^{(P')} \frac{1}{\sqrt{M_{q\bar{q}}^2 M'_{q\bar{q}}{}^2}}. \end{aligned} \quad (23)$$

Finally, recall that the double spectral density of the amplitude $A_{\mu\nu}(P, P', n)$ is calculated by placing all particles in the intermediate mass-on-shell states.

Notice that the amplitude A_T can be directly isolated from $A_{\mu\nu}$. Namely, setting $\mu, \nu = a, b = 1, 2$ and isolating the term $-g_{\mu\nu} \rightarrow \delta_{ab}$, one obtains A_T

$$A_{ab}(P, P', n) = \delta_{ab} A_T + O(\kappa_a \kappa_b), \quad (24)$$

since $\vec{\kappa}$ is the only vector with the components in the transverse plane. In the next Section we perform a detailed consideration of $A_{L,T}$.

III. SPECTRAL REPRESENTATION OF THE AMPLITUDES

The amplitudes of the reactions are given by the diagrams of Fig 1. First, we shall consider separately the upper quark-loop block and then take into account its interaction with a nucleon through the Pomeron exchange. We shall discuss in parallel the cases of the transverse and longitudinal polarizations of the initial photon and outgoing vector meson (photon). As before, we concentrate ourselves on the reaction $\gamma^*(Q^2)p \rightarrow Vp$ keeping in mind that for $\gamma^*(Q^2)p \rightarrow \gamma^*(Q^2)p$ the formulas are written analogously.

A. The block of the photon and vector meson interaction with the BFKL Pomeron

The Pomeron is attached to the photon and the vector meson through the quark loop diagrams of Fig. 1. We consider separately the cases when both Reggeized gluons are attached to the same and to different quarks in the loop.

1. The gluon ladder attached to a single constituent

The diagram for this subprocess is shown in Fig 2a. The analytical spectral representation for this quark-loop diagram has the following structure

$$A_{L,T}^I = \int \frac{dM_{q\bar{q}}^2}{\pi} G_\gamma(M_{q\bar{q}}^2) \frac{d\Phi_2(P; k_1, k_2)}{M_{q\bar{q}}^2 - q^2 - i0} \frac{dM'_{q\bar{q}}{}^2}{\pi} \frac{d\Phi_1(P''; k'_1, k_2)}{M'_{q\bar{q}}{}^2 - (q-k)^2 - i0} \frac{dM''_{q\bar{q}}{}^2}{\pi} \frac{d\Phi_1(P'; k'_1, k_2)}{M''_{q\bar{q}}{}^2 - (q-\kappa)^2 - i0} G_V(M''_{q\bar{q}}{}^2) g^2(-1) S_{L,T}^I, \quad (25)$$

where $P^2 = M_{q\bar{q}}^2$, $P'^2 = M_{q\bar{q}}'^2$, $P''^2 = M_{q\bar{q}}''^2$ are the invariant masses squared of the $q\bar{q}$ pairs in the intermediate states and the corresponding phase space factors read

$$\begin{aligned}
d\Phi_2(P; k_1, k_2) &= \frac{1}{2} \frac{d^3 k_1}{(2\pi)^3 2k_{10}} \frac{d^3 k_2}{(2\pi)^3 2k_{20}} (2\pi)^4 \delta^4(P - k_1 - k_2) \\
&= \frac{1}{(4\pi)^2} \frac{dx_1 dx_2}{x_1 x_2} \delta(1 - x_1 - x_2) d^2 k_{1\perp} d^2 k_{2\perp} \delta(\vec{k}_{1\perp} + \vec{k}_{2\perp}) \delta\left(M_{q\bar{q}}^2 - \frac{m_{1\perp}^2}{x_1} - \frac{m_{2\perp}^2}{x_2}\right), \\
d\Phi_1(P''; k_1'', k_2) &= \frac{1}{2} \frac{d^3 k_1''}{(2\pi)^3 2k_{10}''} (2\pi)^4 \delta^4(P'' - k_1'' - k_2) \\
&= \pi \frac{dx_1''}{x_1''} \delta(1 - x_1'' - x_2) d^2 k_{1\perp}'' \delta(\vec{k}_{1\perp}'' + \vec{k}_{\perp} + \vec{k}_{2\perp}) \delta\left(M_{q\bar{q}}''^2 + k_{\perp}^2 - \frac{m_{1\perp}''^2}{x_1''} - \frac{m_{2\perp}^2}{x_2}\right), \\
d\Phi_1(P'; k_1', k_2) &= \frac{1}{2} \frac{d^3 k_1'}{(2\pi)^3 2k_{10}'} (2\pi)^4 \delta^4(P' - k_1' - k_2) \\
&= \pi \frac{dx_1'}{x_1'} \delta(1 - x_1' - x_2) d^2 k_{1\perp}' \delta(\vec{k}_{1\perp}' + \vec{\kappa}_{\perp} + \vec{k}_{2\perp}) \delta\left(M_{q\bar{q}}'^2 + \kappa_{\perp}^2 - \frac{m_{1\perp}'^2}{x_1'} - \frac{m_{2\perp}^2}{x_2}\right). \tag{26}
\end{aligned}$$

Here we have taken into account that k_z is small: the integration over k_z is performed enclosing the integration contour over the pole $(M_{q\bar{q}}''^2 + Q^2 - 2q_z k_z - i0)^{-1}$, that is equivalent to $(M_{q\bar{q}}''^2 + Q^2 - 2q_z k_z - i0)^{-1} \rightarrow -i\pi\delta(M_{q\bar{q}}''^2 + Q^2 - 2q_z k_z)$. As a result, we find

$$\begin{aligned}
A_{L,T}^I &= \frac{1}{4\pi} \int_0^1 \frac{dx}{x(1-x)^3} \int \frac{d^2 k_{2\perp}}{(2\pi)^2} dk_z \frac{G_\gamma(M_{q\bar{q}}^2)}{M_{q\bar{q}}^2 + Q^2} \frac{1}{M_{q\bar{q}}''^2 + Q^2 - 2q_z k_z - i0} \frac{G_V(M_{q\bar{q}}'^2)}{M_{q\bar{q}}'^2 - \mu_V^2} g^2(-1) S_{L,T}^I \\
&= \int_0^1 \frac{dx}{x(1-x)^3} \int \frac{d^2 k_{2\perp}}{(4\pi)^2} \frac{G_\gamma(M_{q\bar{q}}^2)}{M_{q\bar{q}}^2 + Q^2} \frac{G_V(M_{q\bar{q}}'^2)}{M_{q\bar{q}}'^2 - \mu_V^2} \frac{-ig^2}{2q_z} S_{L,T}^I, \tag{27}
\end{aligned}$$

where

$$M_{q\bar{q}}^2 = \frac{m^2 + k_{2\perp}^2}{x(1-x)}, \quad M_{q\bar{q}}''^2 = \frac{m^2 + (\vec{k}_{2\perp} + x\vec{k}_{\perp})^2}{x(1-x)}, \quad M_{q\bar{q}}'^2 = \frac{m^2 + (\vec{k}_{2\perp} + x\vec{\kappa}_{\perp})^2}{x(1-x)}, \quad x \equiv x_2. \tag{28}$$

The spin factor $S_{L,T}^I$ appears due to a decomposition of the trace $S_{\mu\nu}^I$ corresponding to the quark loop of Fig. 2a

$$S_{\mu\nu}^I = \text{Tr} \left(\gamma_\nu (\hat{k}_1' + m) \hat{n} (\hat{k}_1'' + m) \hat{n} (\hat{k}_1 + m) \gamma_\mu (-\hat{k}_2 + m) \right), \tag{29}$$

where \hat{n} , being determined by (10), stands for the vertex of the reggeized gluon-quark coupling [13]. Let us stress once more that all quarks in this expression are mass-on-shell, whereas the photon and the vector meson momenta are mass-off-shell, such that $P^2 = M_{q\bar{q}}^2$ and $P'^2 = M_{q\bar{q}}'^2$. As we have discussed in the previous Section, to obtain the transverse amplitude, i.e. S_T^I , we must set $\mu, \nu = a, b = 1, 2$ and isolate the structure proportional to δ_{ab} . This procedure yields S_T^I in the form

$$S_T^I = -8 \frac{(1-x)}{x} \left[m^2 + (1-2x(1-x)) \vec{k}_{2\perp} \vec{k}_{2\perp}' \right], \tag{30}$$

where $\vec{k}_{2\perp}' = \vec{k}_{2\perp} + x\vec{\kappa}_{\perp}$. Note that the last term in the square brackets is not small, playing significant role in the determination of A_T .

The spin-factor for longitudinal polarization can be calculated performing the convolution with longitudinal polarization vectors of the off-shell photon and vector meson as follows:

$$S_L^I = \frac{\epsilon_L^{(V)}(P'^2) \text{Tr} \left(\gamma_\beta (\hat{k}_1' + m) \hat{n} (\hat{k}_1'' + m) \hat{n} (\hat{k}_1 + m) \gamma_\alpha (-\hat{k}_2 + m) \right) \epsilon_L^{(\gamma)}(P^2)}{P^2 P'^2 \left(\epsilon_L^{(V)}(P'^2) n \right) \left(\epsilon_L^{(\gamma)}(P^2) n \right)}. \tag{31}$$

The calculation of this trace yields the following result

$$S_L^I = -32 \frac{(1-x)}{x} \frac{x^2(1-x)^2}{m^2 + k_{2\perp}'^2 + x(1-x)\kappa_{\perp}^2} \left[m^2 + k_{2\perp}'^2 - (x-1/2) \vec{k}_{2\perp} \vec{\kappa}_{\perp} \right] \rightarrow -32x(1-x)^3. \tag{32}$$

Here we take into account that the last term in the square brackets gives a negligible contribution into the BFKL amplitude.

2. The gluon ladder attached to both constituents

This subprocess is displayed in Fig 2b. Likewise, the triple spectral representation for the corresponding amplitude takes a form:

$$A_{L,T}^{II} = \int \frac{dM_{q\bar{q}}^2}{\pi} G_\gamma(M_{q\bar{q}}^2) \frac{d\Phi_2(P; k_1, k_2)}{M_{q\bar{q}}^2 - q^2 - i0} \frac{dM_{q\bar{q}}'^2}{\pi} \frac{d\Phi_1(P''; k'_1, k_2)}{M_{q\bar{q}}'^2 - (q - k)^2 - i0} \frac{dM_{q\bar{q}}'^2}{\pi} \frac{d\Phi_1(P'; k'_1, k'_2)}{M_{q\bar{q}}'^2 - (q - \kappa)^2 - i0} G_V(M_{q\bar{q}}'^2) g^2(-1) S_{L,T}^{II}. \quad (33)$$

Now the phase space factors read

$$\begin{aligned} d\Phi_2(P; k_1, k_2) &= \frac{1}{(4\pi)^2} \frac{dx_1 dx_2}{x_1 x_2} \delta(1 - x_1 - x_2) d^2 k_{1\perp} d^2 k_{2\perp} \delta(\vec{k}_{1\perp} + \vec{k}_{2\perp}) \delta\left(M_{q\bar{q}}^2 - \frac{m_{1\perp}^2}{x_1} - \frac{m_{2\perp}^2}{x_2}\right), \\ d\Phi_1(P''; k'_1, k_2) &= \pi \frac{dx'_1}{x'_1} \delta(1 - x'_1 - x_2) d^2 k'_{1\perp} \delta(\vec{k}'_{1\perp} + \vec{k}_\perp + \vec{k}_{2\perp}) \delta\left(M_{q\bar{q}}'^2 + k_\perp^2 - \frac{m_{1\perp}^2}{x'_1} - \frac{m_{2\perp}^2}{x_2}\right), \\ d\Phi_1(P'; k'_1, k'_2) &= \pi \frac{dx'_2}{x'_2} \delta(1 - x'_1 - x'_2) d^2 k'_{2\perp} \delta(\vec{k}'_{1\perp} + \vec{\kappa}_\perp + \vec{k}'_{2\perp}) \delta\left(M_{q\bar{q}}'^2 + \kappa_\perp^2 - \frac{m_{1\perp}^2}{x'_1} - \frac{m_{2\perp}^2}{x'_2}\right). \end{aligned} \quad (34)$$

This time the expressions for the invariants $M_{q\bar{q}}^2, M_{q\bar{q}}'^2, M_{q\bar{q}}'^2$ take a form:

$$M_{q\bar{q}}^2 = \frac{m^2 + k_{2\perp}^2}{x(1-x)}, \quad M_{q\bar{q}}'^2 = \frac{m^2 + (\vec{k}_{2\perp} + (1-x)\vec{k}_\perp)^2}{x(1-x)}, \quad M_{q\bar{q}}'^2 = \frac{m^2 + (\vec{k}_{2\perp} + \vec{k}_\perp - x\vec{\kappa}_\perp)^2}{x(1-x)}, \quad x \equiv x_1. \quad (35)$$

Performing the integration over k_z we come to the expression:

$$A_{q\bar{q}}^{II} = \int_0^1 \frac{dx}{x^2(1-x)^2} \int \frac{d^2 k_{2\perp}}{(4\pi)^2} \frac{G_\gamma(M_{q\bar{q}}^2)}{M_{q\bar{q}}^2 + Q^2} \frac{G_V(M_{q\bar{q}}'^2)}{M_{q\bar{q}}'^2 - \mu_V^2} \frac{-ig^2}{2q_z} S_{L,T}^{II}. \quad (36)$$

The quark loop trace for the diagram of Fig. 2b reads

$$S_{\mu\nu}^{II} = Sp \left(\gamma_\nu (\hat{k}'_1 + m) \hat{n} (\hat{k}_1 + m) \gamma_\mu (-\hat{k}_2 + m) \hat{n} (-\hat{k}'_2 + m) \right). \quad (37)$$

Again, setting $\mu, \nu = a, b = 1, 2$ and isolating the factor proportional to the δ_{ab} yield a simple expression:

$$S_T^{II} = 8 \left[m^2 + (1 - 2x(1-x)) \vec{k}_{2\perp} \vec{k}_{2\perp}'' \right], \quad (38)$$

where we have introduced the vector

$$\vec{k}_\perp'' = \vec{k}_{2\perp} + \vec{k}_\perp - x\vec{\kappa}_\perp. \quad (39)$$

For longitudinal polarization the spin factor reads

$$S_L^{II} = \frac{\epsilon_L^{(V)}(P'^2) Sp \left(\gamma_\beta (\hat{k}'_1 + m) \hat{n} (\hat{k}_1 + m) \gamma_\alpha (-\hat{k}_2 + m) \hat{n} (-\hat{k}'_2 + m) \right) \epsilon_L^{(\gamma)}(P^2)}{P^2 P'^2 \left(\epsilon_L^{(V)}(P'^2) n \right) \left(\epsilon_L^{(\gamma)}(P^2) n \right)}. \quad (40)$$

which, after calculating the trace, takes the following form:

$$S_L^{II} = 32 \frac{x^2(1-x)^2}{m^2 + k_{2\perp}'^2} \left[m^2 + k_{2\perp}'^2 + (x - 1/2) \vec{\kappa}_\perp \vec{k}_{2\perp}'' \right] \rightarrow 32x^2(1-x)^2. \quad (41)$$

Here, as in (32), we take into account that the last term in the square brackets gives a small contribution into the BFKL amplitude.

The vertices $G_\gamma(M_{q\bar{q}}^2)$ and $G_V(M_{q\bar{q}}'^2)$ which are used for the calculation are shown in Fig. 3.

B. BFKL-pomeron couplings to the quark loop and nucleon

Now we must attach the quark loop and target nucleon to the BFKL-pomeron amplitude; we face several possible scenarios for this attaching.

1. Pomeron-nucleon coupling

We consider two possible scenarios for the Pomeron attaching to the nucleon target:

- (i) the BFKL Pomeron is transformed first to the soft Pomeron and then this soft Pomeron is attached to the nucleon,
- (ii) the BFKL is directly attached to the nucleon.

The momentum transfer to the Pomeron κ is not large and there is no selection of the small separations along the gluon ladder: while moving from the quark block to the nucleon, the distances between the t channel gluons in the impact parameter space are increasing.

(i) **Soft-Pomeron-nucleon coupling.** If the ladder is rather long (i.e. at large W), the distances between the gluons become the normal hadronic distances, and in this case the Pomeron is no longer the perturbative BFKL but is rather in a soft regime. This soft Pomeron is then attached to the nucleon, and we use the standard soft-Pomeron-nucleon coupling which we denote as $\tilde{g}F_{PNN}(\kappa_\perp^2)$. Within this scenario and following to the prescription of refs. [5,6,14,15], we write the amplitude of Fig. 1a for the case, when both Reggeized gluons are attached to the same quark (or antiquark):

$$\begin{aligned}
A_{L,T}^{BFKL-q}(\gamma^* p \rightarrow Vp) &= -\frac{i}{2} \int_0^1 \frac{dx}{x^2(1-x)^2} \int \frac{d^2 k_{2\perp}}{(2\pi)^2} \frac{d^2 k_\perp}{(2\pi)^2} \Psi_\gamma(x, k_{2\perp}^2) \Psi_V \left(x, \left(\vec{k}_{2\perp} + x\vec{\kappa}_\perp \right)^2 \right) \\
&\times \frac{x}{1-x} S_{L,T}^I g^2 \int_{-\infty}^{\infty} \frac{d\nu}{(\nu^2 + \frac{1}{4})^2} \left(\frac{W^2}{Q^2 + \mu_V^2} \right)^{\omega(\nu)} \int d^2 \rho_1 d^2 \rho_2 e^{i\vec{k}_\perp \cdot (\vec{\rho}_1 - \vec{\rho}_2)} e^{i\vec{\kappa}_\perp \cdot \vec{\rho}_2} \\
&\times \left(\left[\frac{(\vec{\rho}_1 - \vec{\rho}_2)^2}{\rho_1^2 \rho_2^2} \right]^{\frac{1}{2} + i\nu} - \left[\frac{1}{\rho_1^2} \right]^{\frac{1}{2} + i\nu} - \left[\frac{1}{\rho_2^2} \right]^{\frac{1}{2} + i\nu} \right) \tilde{g}F_{PNN}(\kappa_\perp^2), \tag{42}
\end{aligned}$$

where

$$\Psi_\gamma(x, k_{2\perp}^2) = \frac{G_\gamma(M_{q\bar{q}}^2)}{M_{q\bar{q}}^2 + Q^2}, \quad \Psi_V \left(x, \left(\vec{k}_{2\perp} + x\vec{\kappa}_\perp \right)^2 \right) = \frac{G_V(M_{q\bar{q}}^{\prime 2})}{M_{q\bar{q}}^{\prime 2} - \mu_V^2}, \tag{43}$$

and the invariant masses $M_{q\bar{q}}^2$, $M_{q\bar{q}}^{\prime 2}$ are given by (28).

The variables $\vec{\rho}_1$ and $\vec{\rho}_2$ are the gluon coordinates in the impact parameter space. The energy dependence of the amplitude is given by the function $\omega(\nu)$:

$$\omega(\nu) = \frac{2\alpha_s C_A}{\pi} \text{Re} \left(\frac{\Gamma'(1)}{\Gamma(1)} - \frac{\Gamma'(\frac{1}{2} + i\nu)}{\Gamma(\frac{1}{2} + i\nu)} \right), \tag{44}$$

with $C_A = N_c = 3$ and $\Gamma(z)$ the Euler Γ -function.

Likewise, the amplitude of Fig. 1b, when the gluons are attached to quark and antiquark, takes the form

$$\begin{aligned}
A_{L,T}^{BFKL-q\bar{q}}(\gamma^* p \rightarrow Vp) &= -\frac{i}{2} \int_0^1 \frac{dx}{x^2(1-x)^2} \int \frac{d^2 k_{2\perp}}{(2\pi)^2} \frac{d^2 k_\perp}{(2\pi)^2} \Psi_\gamma(x, k_{2\perp}^2) \Psi_V \left(x, \left(\vec{k}_{2\perp} + \vec{k}_\perp - x\vec{\kappa}_\perp \right)^2 \right) \\
&\times g^2 S_{L,T}^{II} \int_{-\infty}^{\infty} \frac{d\nu}{(\nu^2 + \frac{1}{4})^2} \left(\frac{W^2}{Q^2 + \mu_V^2} \right)^{\omega(\nu)} \int d^2 \rho_1 d^2 \rho_2 e^{i\vec{k}_\perp \cdot (\vec{\rho}_1 - \vec{\rho}_2)} e^{i\vec{\kappa}_\perp \cdot \vec{\rho}_2} \\
&\times \left(\left[\frac{(\vec{\rho}_1 - \vec{\rho}_2)^2}{\rho_1^2 \rho_2^2} \right]^{\frac{1}{2} + i\nu} - \left[\frac{1}{\rho_1^2} \right]^{\frac{1}{2} + i\nu} - \left[\frac{1}{\rho_2^2} \right]^{\frac{1}{2} + i\nu} \right) \tilde{g}F_{PNN}(\kappa_\perp^2), \tag{45}
\end{aligned}$$

where

$$\Psi_\gamma(x, k_{2\perp}^2) = \frac{G_\gamma(M_{q\bar{q}}^2)}{M_{q\bar{q}}^2 + Q^2}, \quad \Psi_V \left(x, \left(\vec{k}_{2\perp} + \vec{k}_\perp - x\vec{\kappa}_\perp \right)^2 \right) = \frac{G_V(M_{q\bar{q}}^{\prime 2})}{M_{q\bar{q}}^{\prime 2} - \mu_V^2}, \tag{46}$$

and the invariant masses $M_{q\bar{q}}^2$ and $M'_{q\bar{q}}^2$ are given by (35).

The nucleon-Pomeron coupling $\tilde{g}F_{PNN}(\vec{\kappa}_\perp^2)$ can be well approximated assuming $F_{PNN}(\kappa_\perp^2) = e^{-B\kappa_\perp^2}$ with $B \simeq 2.5 \text{ GeV}^{-2}$.

The total amplitude is obtained summing the amplitudes of all subprocesses, it takes the form

$$A^{BFKL}(\gamma^*p \rightarrow Vp) = A_{L,T}^{BFKL-q}(\gamma^*p \rightarrow Vp) + A_{L,T}^{BFKL-\bar{q}}(\gamma^*p \rightarrow Vp) + 2 A_{L,T}^{BFKL-q\bar{q}}(\gamma^*p \rightarrow Vp). \quad (47)$$

Some important cancellations occur in the total amplitude: namely, the terms in the BFKL amplitude proportional to ρ_1 or ρ_2 separately cancel each other. In addition, the term proportional to $(\rho_1 - \rho_2)^2$ in $A_{L,T}^{BFKL-q}$ vanishes, since the k_\perp integration yields $\delta(\rho_1 - \rho_2)$.

Finally, we come to the following representation of the total amplitude of the diffractive vector meson production

$$\begin{aligned} A_{L,T}^{BFKL}(\gamma^*p \rightarrow Vp) &= -i \int_0^1 dx \int_0^\infty \frac{d\nu \nu^2}{(\nu^2 + \frac{1}{4})^2} \left(\frac{W^2}{Q^2 + \mu_V^2} \right)^{\omega(\nu)} \\ &\times \int d^2\rho_1 d^2\rho_2 \exp[i\vec{\kappa}_\perp(\vec{\rho}_1 x + \vec{\rho}_2(1-x))] \left[\frac{(\vec{\rho}_1 - \vec{\rho}_2)^2}{\rho_1^2 \rho_2^2} \right]^{\frac{1}{2}+i\nu} \\ &\times \int \frac{d^2k_{2\perp}''}{(2\pi)^2} \frac{d^2k_{2\perp}}{(2\pi)^2} \Psi_\gamma(x, k_{2\perp}^2) \Psi_V(x, k_{2\perp}^2) \exp\left[i(k_{2\perp}'' - \vec{k}_{2\perp})(\vec{\rho}_1 - \vec{\rho}_2)\right] S_{L,T}^{II} C e^{-B\kappa_\perp^2}. \end{aligned} \quad (48)$$

where $k_{2\perp}''$ is given by (39), and $C = g^2\tilde{g}$ plays a role of the normalization constant.

It is convenient to transform the final expression for the photon and vector meson wave functions to the coordinate representation as follows:

$$\begin{aligned} A_{L,T}^{BFKL}(\gamma^*p \rightarrow Vp) &= -\frac{i}{(2\pi)^2} C e^{-B\kappa_\perp^2} \int_0^1 \frac{dx}{x^2(1-x)^2} \int_0^\infty \frac{d\nu \nu^2}{(\nu^2 + \frac{1}{4})^2} \left(\frac{W^2}{Q^2 + \mu_V^2} \right)^{\omega(\nu)} \\ &\times \int d^2\rho d^2R e^{i\vec{\kappa}_\perp(\vec{R} - (\frac{1}{2}-x)\vec{\rho})} \left[\frac{\rho^2}{(\vec{R} + \frac{\vec{\rho}}{2})^2 (\vec{R} - \frac{\vec{\rho}}{2})^2} \right]^{\frac{1}{2}+i\nu} F_{L,T}(x, \rho^2), \end{aligned} \quad (49)$$

where $\vec{R} = (\vec{\rho}_1 + \vec{\rho}_2)/2$ and $\vec{\rho} = \vec{\rho}_1 - \vec{\rho}_2$. The functions $F_{L,T}(x, \rho^2)$ are defined as follows:

$$F_L(x, \rho^2) = 32 x^2(1-x)^2 \Phi_V^{(0)}(x, \rho^2) \Phi_\gamma^{(0)}(x, \rho^2), \quad (50)$$

$$F_T(x, \rho^2) = 8 \left(m^2 \Phi_V^{(0)}(\rho^2) \Phi_\gamma^{(0)}(\rho^2) + 2(1-2x(1-x)) \Phi_V^{(1)}(x, \rho^2) \Phi_\gamma^{(1)}(x, \rho^2) \right), \quad (51)$$

where

$$\Phi^{(n)}(\rho^2) = \int_0^\infty dk k^{n+1} \Psi(k^2) J_n(k\rho). \quad (52)$$

(ii) **BFKL-pomeron-nucleon coupling.** One could also imply another scenario for the Pomeron coupling to nucleon target. Indeed, if the gluon ladder is rather short and BFKL Pomeron is not transformed into a soft one, the amplitude of the vector meson production takes the following form:

$$\begin{aligned} A_{L,T}^{BFKL}(\gamma^*p \rightarrow Vp) &= -i \int_0^1 \frac{dx}{x^2(1-x)^2} \int_0^\infty \frac{d\nu \nu^2}{(\nu^2 + \frac{1}{4})^2} \left(\frac{W^2}{Q^2 + \mu_V^2} \right)^{\omega(\nu)} \\ &\times \int d^2\rho d^2R e^{i\vec{\kappa}_\perp(\vec{R} - (\frac{1}{2}-x)\vec{\rho})} \left[\frac{\rho^2}{(\vec{R} + \frac{\vec{\rho}}{2})^2 (\vec{R} - \frac{\vec{\rho}}{2})^2} \right]^{\frac{1}{2}+i\nu} \frac{1}{(2\pi)^2} C A_N(\nu, \vec{\kappa}_\perp) S_{L,T}^{II}. \end{aligned} \quad (53)$$

Here we have introduced the quantity

$$\begin{aligned}
A_N(\nu, \vec{\kappa}_\perp) = & \int d^2\rho'_1 d^2\rho'_2 \left(\left[\frac{(\vec{\rho}'_1 - \vec{\rho}'_2)^2}{\rho'^2_1 \rho'^2_2} \right]^{\frac{1}{2} - i\nu} - \left[\frac{1}{\rho'^2_1} \right]^{\frac{1}{2} - i\nu} - \left[\frac{1}{\rho'^2_2} \right]^{\frac{1}{2} - i\nu} \right) \exp \left(i\vec{\kappa}_\perp \frac{\vec{\rho}'_1 + \vec{\rho}'_2}{2} \right) \\
& \times \left(\exp \left(-\frac{2(\rho'^2_1 + \rho'^2_2)}{3 \langle r^2 \rangle} \right) - \delta(\vec{\rho}'_1 - \vec{\rho}'_2) \frac{3}{2} \pi \langle r^2 \rangle \exp \left(-\frac{(\vec{\rho}'_1 + \vec{\rho}'_2)^2}{6 \langle r^2 \rangle} \right) \right), \quad (54)
\end{aligned}$$

with $\langle r^2 \rangle = 0.8 \text{ fm}^2$. This form of the nucleon wave function corresponds to the exponential dependence of the nucleon-pomeron vertex $\exp(-B\kappa_\perp^2)$ with $B \simeq 2 \text{ GeV}^{-2}$.

However, numerically the amplitude turns out to be poorly sensitive to the details of the mechanism of the pomeron attachment to the nucleon target: namely, all the results obtained within the assumption of a direct attachment of the BFKL pomeron to the nucleon coincide, within a few percent accuracy, with the results obtained under the assumption that the transition from the BFKL regime to the soft one occurs before attaching to the nucleon.

2. Pomeron coupling to the quark loop

Before, following refs. [5,6,14,15], we have determined the W -dependence using the factor $[W^2/(Q^2 + \mu_V^2)]^{\omega(\nu)}$: here the variables Q^2 and μ_V^2 are external with respect to the quark loop. In writing spectral representation for the quark loop, the more self-consistent procedure is to use the internal variables, $M_{q\bar{q}}^2$ and $M'_{q\bar{q}}{}^2$, instead of external ones. For this scheme, we should replace in the above formulas:

$$\left(\frac{W^2}{Q^2 + \mu_V^2} \right)^{\omega(\nu)} \rightarrow \left(\frac{W^2}{M_{q\bar{q}}^2 + M'_{q\bar{q}}{}^2} \right)^{\omega(\nu)} \quad (55)$$

The BFKL-equation with internal variables for the dimensionless W -dependent factor was considered in [12]. We perform calculations for both variants, using both external and internal variables.

3. Numerical calculations

Numerical calculations have been performed using the Monte-Carlo simulation program VEGAS [16]. Integration limits related to $M_{q\bar{q}}^2$ and $M'_{q\bar{q}}{}^2$ depend on Q^2 , namely, $M_{q\bar{q}}^2 \leq 100 Q^2$ (the increase of the upper limit does not change the result). The integration over ρ is performed up to $\rho \leq 5 \text{ fm}$.

IV. RESULTS

To study the onset of the hard region dominance in diffractive processes initiated by the photon with the increase of Q^2 , we consider in parallel the following reactions

$$\gamma_L^*(Q^2)p \rightarrow \gamma_L^*(Q^2)p, \quad (56)$$

$$\gamma_T^*(Q^2)p \rightarrow \gamma_T^*(Q^2)p \quad (57)$$

and

$$\gamma_L^*(Q^2)p \rightarrow \rho_L^0 p, \quad (58)$$

$$\gamma_T^*(Q^2)p \rightarrow \rho_T^0 p. \quad (59)$$

The main ingredients of the calculation of the amplitudes of these reactions are the consideration of the hard quark block and the pomeron amplitude and its attachment to the nucleon target.

The processes (56), (57) can be reliably described at large Q^2 , because the photon wave function is known due to the analysis of ref. [2]. The corresponding vertex $G_\gamma(M_{q\bar{q}}^2)$ is shown in Fig. 3a. Notice that a reliability of calculating the quark loop diagram $\gamma^*(Q^2) \rightarrow q\bar{q} \rightarrow \gamma^*(Q^2)$ is the main motivation for the study of the processes (56), (57). The calculated cross section of the reaction (56) within the amplitude determined by Eq. (49) is shown in Fig. 4 by solid

lines. The amplitude A_L determines $d\sigma/d\kappa_{\perp}^2(\gamma_L^*(Q^2)p \rightarrow \gamma_L^*(Q^2)p)$ (Figs. 4b,c,d): the integrated κ_{\perp}^2 -distribution over the region $\kappa_{\perp, min}^2 \leq \kappa_{\perp}^2 \leq 1 \text{ GeV}^2$ yields $\sigma(\gamma_L^*(Q^2)p \rightarrow \gamma_L^*(Q^2)p)$ (the cutting parameter $\kappa_{\perp, min}^2 = 0.05 \text{ GeV}^2$ is introduced to avoid the divergence of the BFKL-amplitude at $\kappa_{\perp}^2 = 0$).

For illustration of the role of low- $M_{q\bar{q}}$ region in the realistic photon vertex, $G_{\gamma}(M_{q\bar{q}}^2)$, we also perform calculations of the cross section $\gamma_L^*(Q^2)p \rightarrow \gamma_L^*(Q^2)p$ with $G_{\gamma}(M_{q\bar{q}}^2) = 1$, Fig. 5.

Results for the reaction (56) are shown in Fig. 6.

An essential ingredient of the amplitude of the reaction is the description of the pomeron-exchange block. A realistic picture of the pomeron block is the following: small average transverse separations in the gluon ladder selected by the quark loop increase as a result of the t -channel evolution, and the hard pomeron transforms into a soft one along the gluon ladder. This feature is taken into account by using the pomeron-proton coupling as given in Eq. (49). The corresponding results are shown in Figs. 4-8.

Nevertheless, for the sake of illustration we also performed calculations for another variant, with a prompt attachment of the BFKL-pomeron directly to the target nucleon, see Eq. (54). The results for the W -dependence, after renormalizing the coupling constant $C = g^2\tilde{g}$, are practically the same for both variants so we do not present separately the results obtained by using Eq. (54).

We also study different possibilities of choosing the scale of the W^2 -dependence of the BFKL amplitude and consider the two possibilities: (1) $W^2/(Q^2 + \mu_V^2)$ and (2) $W^2/(M_{q\bar{q}}^2 + M_{q\bar{q}}^2)$, see Eq. (55). Calculations with the variant (2) are shown in Fig. 7. One observes a sizeable sensitivity of the calculated cross sections to the choice of the W^2 -scale.

The reactions of the ρ^0 -meson diffractive production are extensively studied both experimentally and theoretically (see, e.g., [15,17,18] and references therein). However, the calculation of the quark-loop diagram $\gamma^*(Q^2) \rightarrow q\bar{q} \rightarrow \rho^0$ turns out to be rather ambiguous due to the uncertainty in the large- $M_{q\bar{q}}$ behaviour of the ρ -meson vertex $G_{\rho}(M_{q\bar{q}}^2)$. Because of that, we analyze several possibilities of the large- $M_{q\bar{q}}$ behaviour of the vertex $G_{\rho}(M_{q\bar{q}}^2)$. The results for the two variants, namely (1) $G_{\rho}(M_{q\bar{q}}^2) \sim M_{q\bar{q}}^{-2}$ and (2) $G_{\rho}(M_{q\bar{q}}^2) \sim \text{const}$ (see Fig. 3b), are represented by solid lines in Fig. 8.

In order to check the consistency of our initial assumption that at the considered Q^2 and W the amplitude is dominated by the small separations of the gluons in the ladder, and thus the BFKL form of the kernel should be used we have also performed calculations introducing explicitly a θ -function cut into the BFKL-amplitude integrand of (49): this θ -function measures an actual contribution of the hard region of separations smaller than 0.2 fm:

$$d^2\rho \rightarrow d^2\rho \theta(0.2 \text{ fm} - \rho). \quad (60)$$

The cross sections constrained by (60) are shown in Figs. 4, 5, 6, 7 and 8 by dashed lines: one can see that for all reactions the selection of small distances, if any, occurs very slowly with the increase of Q^2 . Only at $Q^2 > 100 \text{ GeV}^2$, the 80% of the cross sections are actually gained in the hard region. Thus we conclude that the dominance of the hard region cannot be expected earlier than at $Q^2 > 50 - 100 \text{ GeV}^2$.

Let us notice that the situation with the diffractive production by the hard photon in the region of $Q^2 \leq 100 \text{ GeV}^2$ turns out to be quite similar to the situation with the elastic meson form factor at $Q^2 \leq 10\text{-}20 \text{ GeV}^2$: in the latter case one can expect the dominance of the hard-scattering mechanism (which is proved to be the dominant mechanism at asymptotically large Q^2) also at Q^2 of several GeV^2 . Assuming such dominance at several Q^2 one determines the soft wave function of the pion at low normalization point by describing the data on the form factor and finds for this wave function a double-humped form [7]. However, analyzing the content of the calculated form factor, one finds that the bulk of the contribution actually comes from the end-point region where the hard-scattering mechanism is not applicable but rather the Feynman mechanism works [8]. This analysis shows that the perturbative treatment of the form factor at several GeV^2 is not consistent (or at least the perturbative mechanism cannot give a bulk of the form factor) and that the soft physics actually dominates in the kinematical region $Q^2 \leq 20 \text{ GeV}^2$.

Likewise, we have found that the assumption of the BFKL form of the pomeron kernel actually yields in the region of $Q^2 \leq 100 \text{ GeV}^2$ the cross section which is at 80% level gained in the region of *large* transverse separations in the quark loop. The latter are equal to gluon separations at the top of the gluon ladder which thus turns out to be in the soft regime just from the top. Therefore, similar to the elastic form factor case, we have to conclude that the perturbative treatment in this range of Q^2 is not consistent and that rather the soft pomeron should be used.

Considering the region of $Q^2 \geq 100 \text{ GeV}^2$, we have observed that the dominance of the region of small separations in the quark loop depends on the subtle details of the calculation procedure: namely, some of the variants of the calculation discussed here yield the cross sections $\sigma(W, Q^2)$ and $(\sigma(W, Q^2))_{\rho < 0.2 \text{ fm}}$ which differ even at very large Q^2 : this means that the region $\rho > 0.2 \text{ fm}$ still gives a non-vanishing contribution even at asymptotically large Q^2 .

More detailed and technical explanation is as follows:

It might happen that the spectral representation of the quark loop was superconvergent, i.e. the factor $M_{q\bar{q}}^2$ in the denominator was not essential for the convergence of the integral. Then the denominator $(M_{q\bar{q}}^2 + Q^2)^{-1}$ could be

safely expanded in powers of $1/Q^2$, namely, $(M_{q\bar{q}}^2 + Q^2)^{-1} \rightarrow 1/Q^2$. Then one would not observe any selection of the hard region even at asymptotically large Q^2 : the Q^2 dependence would just factorize and the integrals would be still dominated by typical hadronic scales.

In the reactions (56) and (57), choosing the scale $W^2/(Q^2 + \mu_V^2)$ for the W^2 -dependence, one observes the cross sections $\sigma(W, Q^2)$ and $(\sigma(W, Q^2))_{\rho < 0.2 \text{ fm}}$ to be very close to each other at $Q^2 \geq 100 \text{ GeV}^2$ (see Figs. 4 and 6). This means that the spectral representations are not superconvergent and thus the hard photon actually selects small distances in the quark loop and, as a result, the top of the pomeron ladder is in the perturbative regime.

The introduction of the scale-factor $W^2/(M_{q\bar{q}}^2 + M_{q\bar{q}}^{\prime 2})$ provides a superconvergence of the spectral integrals, thus making the cross sections $\sigma(W, Q^2)$ and $(\sigma(W, Q^2))_{\rho < 0.2 \text{ fm}}$ different even at $Q^2 \rightarrow \infty$. In other words, small separations are not selected in this variant of calculation even at asymptotically large Q^2 .

The similar situation is observed in the diffractive vector meson production reactions (58) and (59).

Namely, for the variant $G_\rho(M_{q\bar{q}}^2) \sim \text{Const}$ at $M_{q\bar{q}}^2 \rightarrow \infty$ (see Fig. 8) the integrals are not superconvergent and thus small separations dominate the amplitude at large Q^2 . The only quantitative difference with the photon production case is that the proximity of cross sections $\sigma(W, Q^2)$ and $(\sigma(W, Q^2))_{\rho < 0.2 \text{ fm}}$, with the scale $W^2/(Q^2 + \mu_V^2)$, comes later with the increase of Q^2 .

For the variant $G_\rho(M_{q\bar{q}}^2) \sim 1/M_{q\bar{q}}^2$ the spectral representations are superconvergent and there is no dominance of the small separations in the quark loop even at asymptotically large Q^2 ; correspondingly, the contribution of distances $\rho > 0.2 \text{ fm}$ is always important in this variant.

Low- $M_{q\bar{q}}$ structure of $G_\rho(M_{q\bar{q}}^2)$ and $G_\gamma(M_{q\bar{q}}^2)$ is very important in realistic treatment of reactions $\gamma^*(Q^2)p \rightarrow Vp$ and $\gamma^*(Q^2)p \rightarrow \gamma^*(Q^2)p$: it is seen in comparing Figs. 4 and 5. Low- $M_{q\bar{q}}$ structure is essential for different behaviour of $d\sigma/d\kappa_\perp^2(W, Q^2, \kappa_\perp^2)$ and $(d\sigma/d\kappa_\perp^2(W, Q^2, \kappa_\perp^2))_{\rho < 0.2 \text{ fm}}$ in the region of small κ_\perp^2 at $Q^2 \sim 20 - 50 \text{ GeV}^2$.

Let us discuss now in a more detail the role of large and small $M_{q\bar{q}}^2$ in the formation of cross sections initiated by $\gamma_L^*(Q^2)$ and $\gamma_T^*(Q^2)$. The distinction of corresponding cross sections is due to a different structure of the spin-dependent factors, S_T^{II} and S_L^{II} , related to the loop diagrams (see (38) and (41): for the case of longitudinal polarization the spin dependent factor is $S_L^{II} \sim x^2(1-x^2)$, whereas $S_T^{II} \neq 0$ at $x \rightarrow 0$ or $(1-x) \rightarrow 0$. Therefore, since $M_{q\bar{q}}^2 = m_\perp^2/x/(1-x)$, the large masses, i.e. the regions $x \sim 0$ and $(1-x) \sim 0$, become dominant for the reactions $\gamma_T^*(Q^2) \rightarrow \gamma_\pi^*(Q^2)$ and $\gamma_T^*(Q^2) \rightarrow \rho_T^0$, but there is no such dominance for the reactions with $\gamma_L^*(Q^2)$. This means that in the transitions $\gamma_L^*(Q^2) \rightarrow \gamma_\pi^*(Q^2)$ $\gamma_L^*(Q^2) \rightarrow \rho_L^0$ small $M_{q\bar{q}}^2$ or large interquark separations contribute considerably. The realistic photon wave function also enhances the role of the large interquark distances, thus resulting in a different behaviour of the cross sections $d\sigma/d\kappa_\perp^2(\gamma_L^*(Q^2)p \rightarrow \gamma_L^*(Q^2)p)$ and $d\sigma/d\kappa_\perp^2(\gamma_L^*(Q^2)p \rightarrow \gamma_L^*(Q^2)p)_{\rho < 0.2 \text{ fm}}$ at $\kappa_\perp^2 \sim 0.1 \text{ GeV}^2$ in the region $Q^2 \sim 20 - 50 \text{ GeV}^2$ (compare Fig. 4c and Fig. 5d).

V. CONCLUSION

The performed calculations demonstrate that a selection of small distances by the virtual photon $\gamma^*(Q^2)$ with the increase of Q^2 have the following features: First, it strongly depends on the choice of the W^2 -scale. Second, it proceeds very slowly: in the quark loops for the transitions $\gamma^*(Q^2) \rightarrow \gamma^*(Q^2)$ and $\gamma^*(Q^2) \rightarrow \rho^0$ the soft interquark distances $\rho > 0.2 \text{ fm}$ clearly dominate the amplitude at $Q^2 < 100 \text{ GeV}^2$.

The situation here is quite similar to that of meson elastic form factors, where the pQCD regime starts to dominate at $Q^2 > 50 \text{ GeV}^2$ only (see the results for the pion and transition form factors in [1,2] and a general discussion in [8]). From this point of view, the results of our analysis [1,2] and the present paper seem to be quite consistent with each other.

The late onset of the pQCD in the reaction $\gamma^*(Q^2)p \rightarrow Vp$ means that it is the Strong-QCD pomeron that actually works at $Q^2 \leq 100 \text{ GeV}^2$, thus exposing an intriguing situation with vector meson electroproduction processes.

The matter is that the W -dependence of the photoproduction reactions ($Q^2 = 0$) in the region $W \sim 10 - 200 \text{ GeV}$ is rather flat, similar to that in hadronic processes like $\pi p \rightarrow \pi p$. However, the reaction $\gamma^*(Q^2)p \rightarrow Vp$ at $Q^2 \sim 10 - 20 \text{ GeV}^2$ demonstrates a different W -dependence: namely, the cross sections increase as $W^{2\Delta}$ with $\Delta \approx 0.3$. There might be an attractive possibility to refer this growth to the change of the pomeron regime from the Strong-QCD one in the first case to the BFKL pomeron in the second one.

However the results of our analysis show that the BFKL pomeron cannot be seen in the diffractive production in the region $Q^2 \leq 100 \text{ GeV}^2$. Therefore, a theoretical explanation of the change of the W dependence lies in better understanding of properties of the Strong-QCD pomeron. One of the possibilities is to explain this change of the W dependence by a complicated 'heterogeneous' structure of the Strong-QCD pomeron, when its different components reveal themselves at $Q^2 \sim 0$ and $Q^2 \sim 10 \text{ GeV}^2$.

For example, one may suggest the following scenarios for the Strong-QCD pomeron:

- In the reactions with $Q^2 \sim 0$ as well as hadronic processes $\pi p \rightarrow \pi p$ or $pp \rightarrow pp$, the amplitude is governed by the pomeron with intercept close to unity: $j = 1 + \Delta$, with $\Delta \simeq 0.1$ (KTDL-pomeron [19]). In this case, the KTDL-pomeron contribution must vanish at $Q^2 \sim 10 \text{ GeV}^2$ leaving the leading role to a new pole with a larger intercept, $\Delta_{new \text{ pole}} \simeq 0.3$ [20].
- In the reactions with $Q^2 \sim 0$ as well as hadronic processes $\pi p \rightarrow \pi p$ or $pp \rightarrow pp$, the amplitude is determined by multiple primary-pomeron-induced rescatterings in the direct channel [21,22]. A slow growth of the amplitudes at $W \sim 10 - 200 \text{ GeV}$, $\Delta_{effective} \simeq 0.1$, occurs at rather large value of the primary pomeron intercept, $\Delta_{primary \text{ pomeron}} \simeq 0.3$ [22]. In this scenario, in order to obtain the growth of the electroproduction amplitudes observed in the experiment, $\sim W^{0.6}$, the multiple rescatterings should die with the increase of Q^2 in such a way that at moderately large Q^2 only the one-pomeron exchange survives, leading to the amplitude growth $\sim W^{2\Delta_{primary \text{ pomeron}}}$.

However a detailed consideration of the Strong-QCD pomeron is beyond the scope of this article and we leave this intriguing subject to other publications.

VI. ACKNOWLEDGMENTS

We are grateful to G. Korchemsky for helpful comments. This work was supported in part by RFBR under grant 98-02-17236.

-
- [1] V.V. Anisovich, D.I. Melikhov, and V.A. Nikonov, Phys. Rev. **D52**, 5295 (1995).
 - [2] V.V. Anisovich, D.I. Melikhov, and V.A. Nikonov, Phys. Rev. **D55**, 2918 (1997);
V.V. Anisovich, D.V. Bugg, D.I. Melikhov, and V.A. Nikonov, Phys. Lett. **B404**, 166 (1997).
 - [3] A.V. Efremov, A.V. Radyushkin, Phys. Lett. **94B**, 45 (1980).
 - [4] S.J. Brodsky, G.P. Lepage, Phys. Rev. **D22**, 2157 (1980).
 - [5] E. A. Kuraev, L. N. Lipatov, V. S. Fadin, Sov. Phys. JETP **44**, 443 (1976);
I. I. Balitsky, L. N. Lipatov, Sov. J. Nucl. Phys. **28**, 822 (1978).
 - [6] L. N. Lipatov, Sov. Phys. JETP **63**, 904 (1986).
 - [7] V.L. Chernyak and A.R.Zhitnitsky, Phys. Rep. **112**, 173 (1984).
 - [8] N. Isgur and C. Llewellyn-Smith, Phys. Lett. **B217**, 535 (1989); Nucl. Phys. **B317**, 526 (1989).
 - [9] CLEO Collaboration, V. Savinov, "A measurement of the form factors of light pseudoscalar mesons at large momentum transfers", hep-ex/9507005 (1995), unpublished;
CELLO Collaboration, H.J. Behrend et al., Z. Phys. **C49** (1991) 401;
TCP/2 γ Collaboration, H. Aihara et al., Phys. Rev. Lett. **64** (1990) 172.
 - [10] Crystall Ball Collaboration, D. Williams et al., Phys. Rev. **D38** (1988) 1365.
 - [11] C. Bebek et al. Phys. Rev. **D13**, 25 (1976); **D17**, 1693 (1978);
S.R. Amendolia et al. Nucl. Phys. **B277**, 169 (1986)
 - [12] V.S. Fadin, L.N. Lipatov, Phys. Lett. **B429**, 127 (1998).
 - [13] G.V. Frolov, V.N. Gribov, L.N. Lipatov, Sov. J. Nucl. Phys. **12**, 543 (1971) .
 - [14] J. Bartels, L.N. Lipatov, J.R. Forshaw, H. Lotter, and M.G. Ryskin, Phys. Lett. **B348**, 589 (1995).
 - [15] J.R. Forshaw and D.A. Ross, *Quantum Chromodynamics and the Pomeron*, Cambridge University Press, 1998.
 - [16] G.P. Lepage, J. Comp. Phys. **27**, 192 (1978).
 - [17] A.D. Martin, M.G. Ryskin, T. Teubner, Phys. Rev. **D55**, 4329 (1997);
I.F. Ginzburg, D.Yu. Ivanov, Phys. Rev. **D54** 5523 (1996);
S.J. Brodsky et al., Phys. Rev. **D50**, 3134 (1994);
N.N. Nikolaev et al., Phys. Lett. **B328** 486 (1994).
 - [18] J. Gayler, in: *Proceedings of the 28th International Conference on High Energy Physics*, edited by Z. Ajduk and A.K. Wroblewski, World Scientific, Singapore, 1997, pp. 608-612.
 - [19] A.B. Kaidalov and K.A. Ter-Martirosyan, Sov. J. Nucl. Phys. **39**, 979 (1984);
A. Donnachie and P.V. Landshoff, Nucl. Phys. **B231** 189 (1984).
 - [20] A. Donnachie and P.V. Landshoff, Phys. Lett. **B437** 408 (1998);
N.N. Nikolaev et al., JETP Lett. **66**, 138 (1997).

- [21] B. Margolis, P. Valin, M. Block, F. Halzen, and R.S. Fletcher, Phys. Rev. D**41** , 978 (1990);
R.S. Fletcher, T.K. Gaisser, and F. Halzen, Phys. Lett. **B298**, 442 (1993);
J. Pumplin, Phys. Lett. **B276**, 517 (1992); **B289**, 449 (1992);
T.T. Chou and C.N. Yang, Phys. Lett. **B244**, 113 (1990).
[22] L.G.Dakhno, "Perturbative QCD-pomeron and high-energy hadronic diffractive cross sections", in: Frontiers in Strong Interactions, Proceedings of VI Blois Workshop, ed. by P.Chiapetta, M.Hagenauer and J.Tran Thanh Van, Edition Frontière, Gif-sur-Ivette, 1995, pp. 189-191;
L.G. Dakhno and V.A. Nikonov, *Hadron Diffractive Processes: the Structure of Soft Pomeron and Color Screening*, hep-ph/9902320, submitted to EPJA.

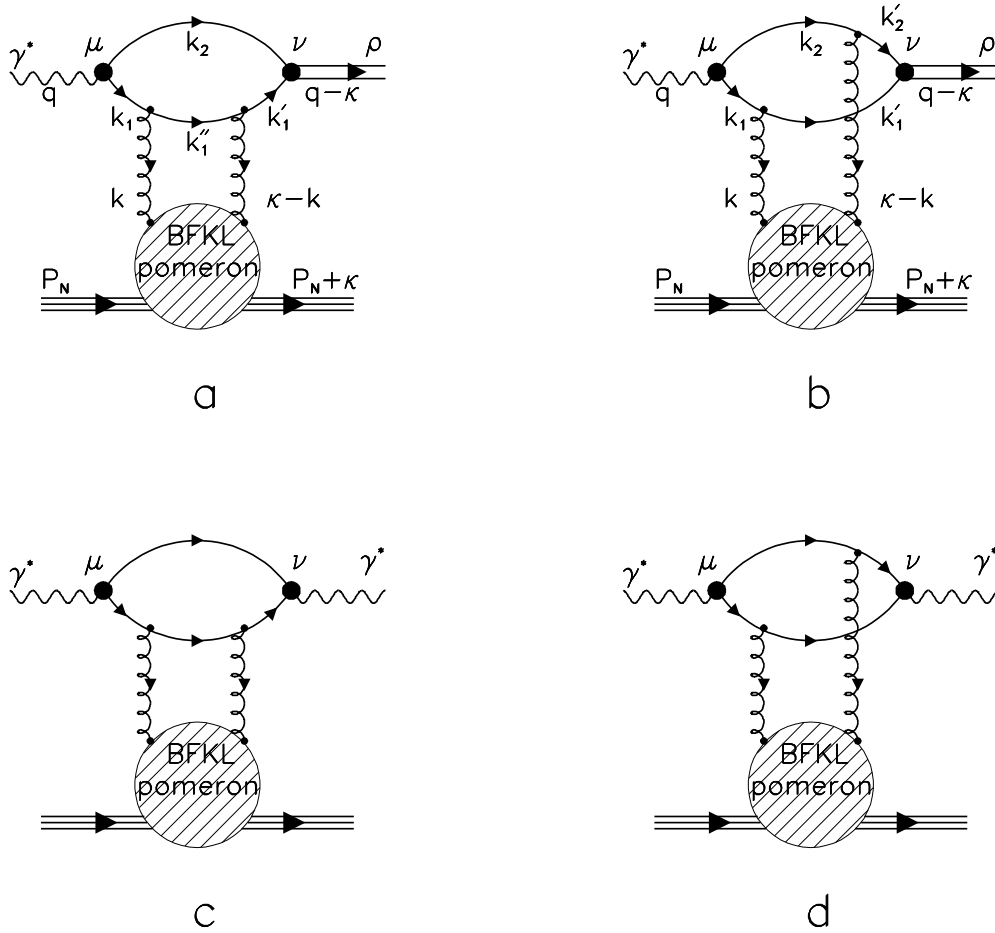


FIG. 1. Diagrams for the processes $\gamma^*(Q^2)p \rightarrow \rho^0 p$ (a,b) and $\gamma^*(Q^2)p \rightarrow \gamma^*(Q^2)p$ (c,d).

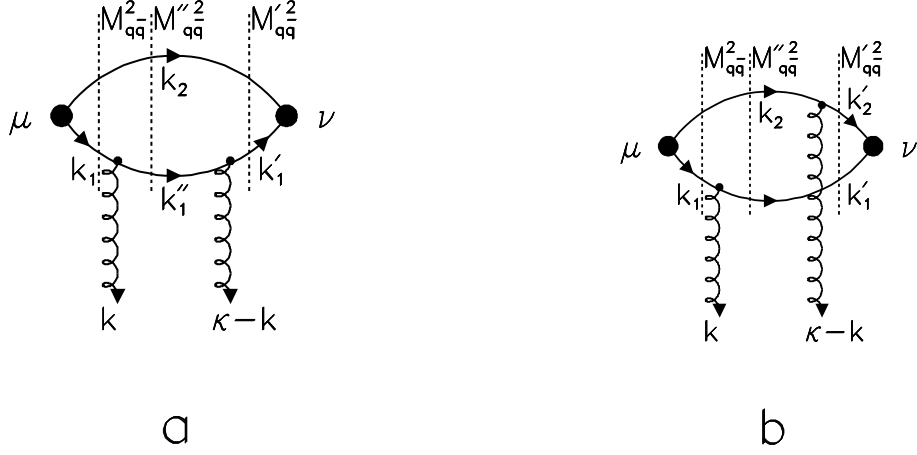


FIG. 2. Quark loop for the case the gluon interaction with a quark (a) and with quark and antiquark (b). Dashed line indicates the cut of a loop related to the spectral integrals.

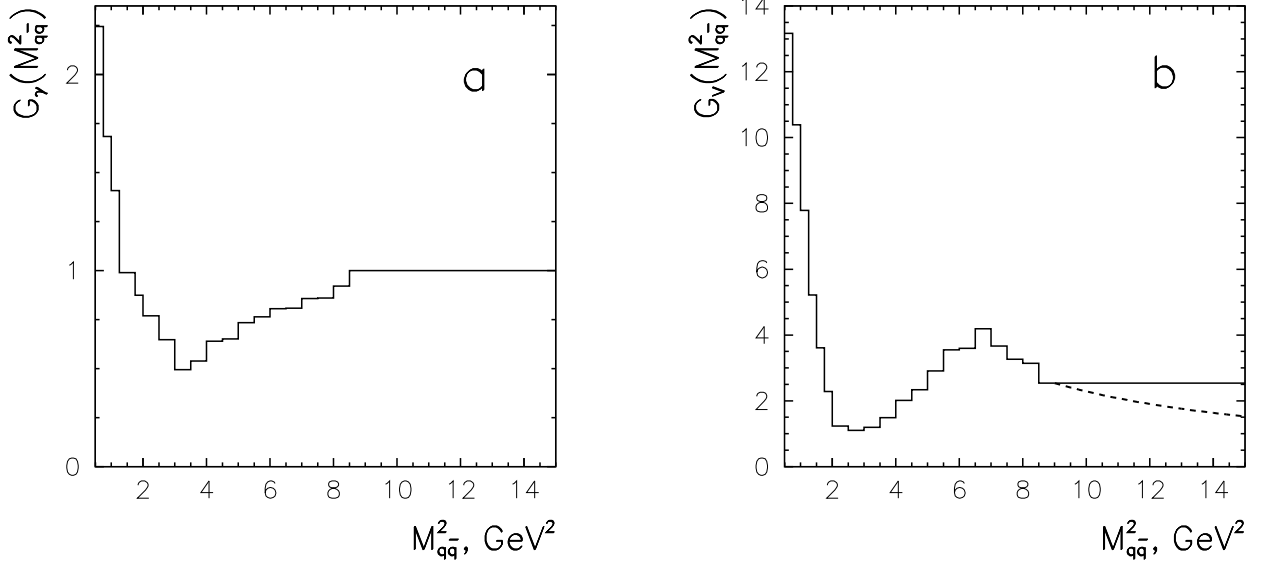


FIG. 3. (a) The vertex $G_\gamma(M_{q\bar{q}}^2)$ found in the analysis of transition form factors $\gamma \rightarrow \pi^0, \eta, \eta'$ in [2]. (b) The ρ -meson vertex function used in the calculation; At $M_{q\bar{q}} > 3$ GeV two variants are shown: I) the decrease $G_\gamma(M_{q\bar{q}}^2) \sim 1/M_{q\bar{q}}^2$ (dashed curve), II) $G_\gamma(M_{q\bar{q}}^2) \sim const$ (solid curve).

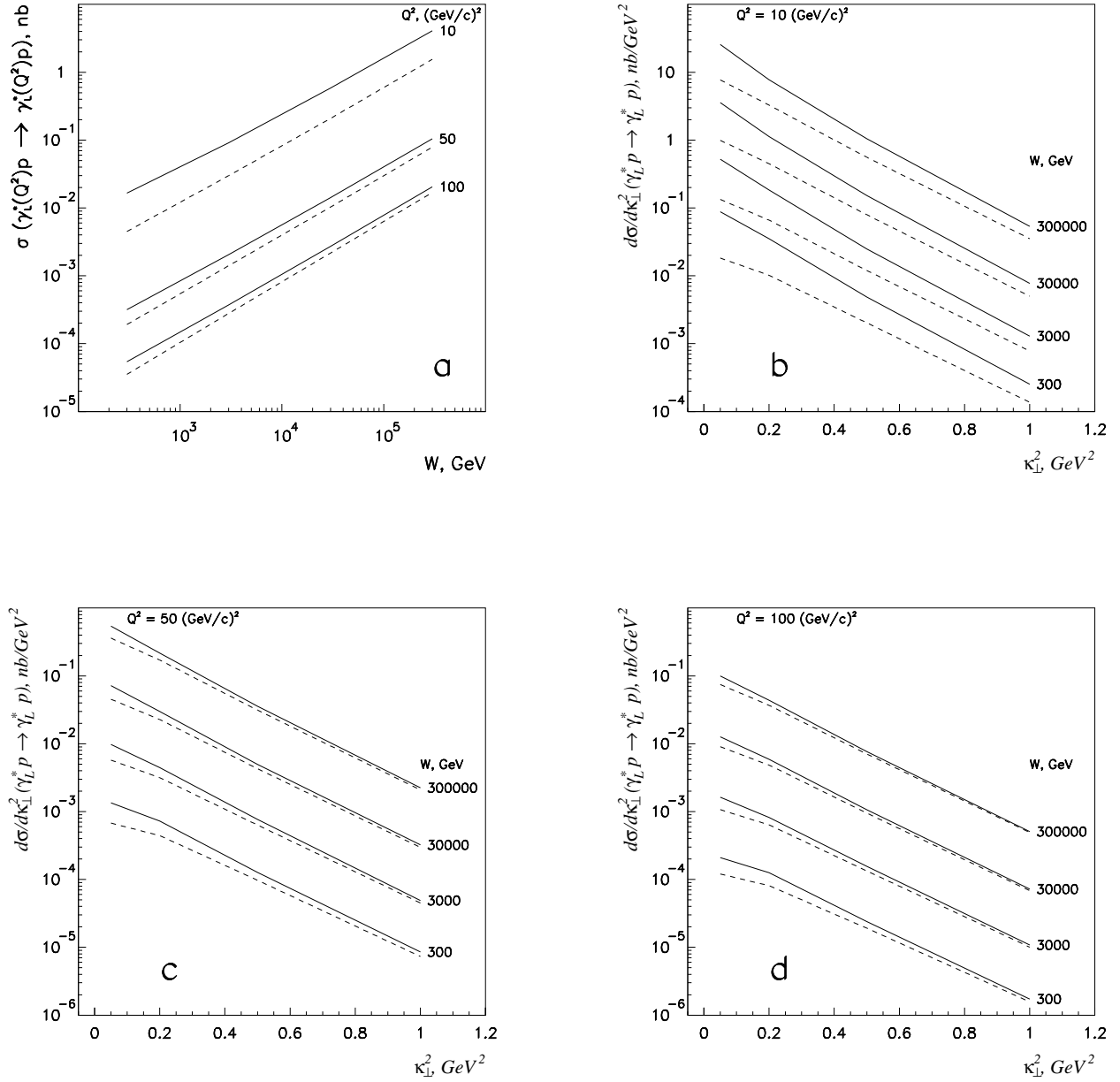


FIG. 4. Cross sections in reaction $\gamma_L^*(Q^2)p \rightarrow \gamma_L^*(Q^2)p$ with the W -scale factor $W^2/(Q^2 + \mu_V^2)$, normalization is fixed by cross section of reaction $\gamma_L^*(Q^2 = 10 \text{ GeV}^2)p \rightarrow \rho_{LP}^0$. Solid curves correspond to $\sigma(W, Q^2)$ (a) and $d\sigma/d\kappa_\perp^2(W, Q^2)$ (b,c,d) calculated without a cut in the quark loop; dashed lines stand for $\sigma(W, Q^2)_{\rho < 0.2 \text{ fm}}$ (a) and $d\sigma/d\kappa_\perp^2(W, Q^2)_{\rho < 0.2 \text{ fm}}$ (b,c,d).

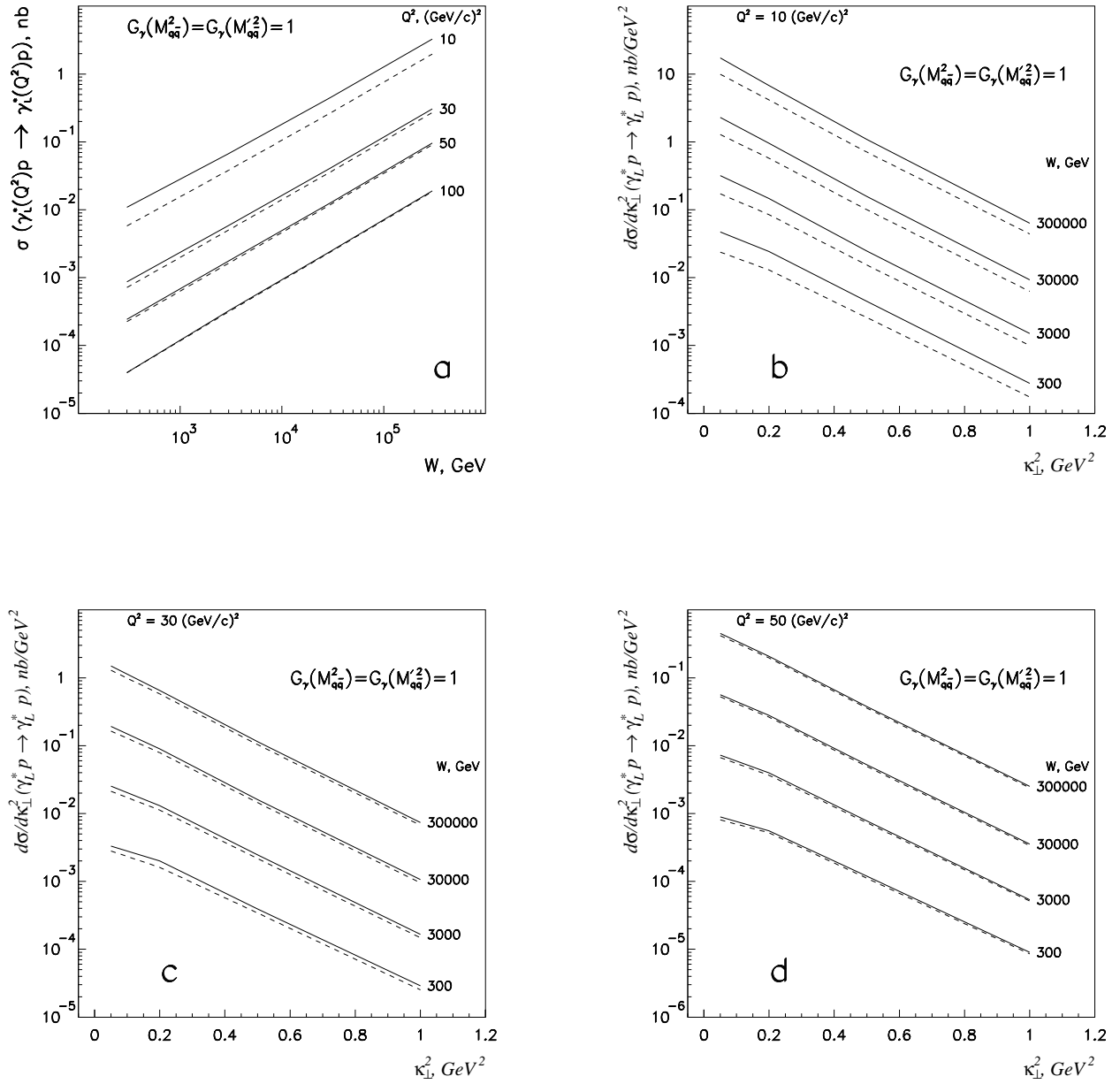


FIG. 5. The same as in Fig. 4, but with $G_\gamma(M_{q\bar{q}}^2) = G_\gamma(M_{q\bar{q}}^2) = 1$.

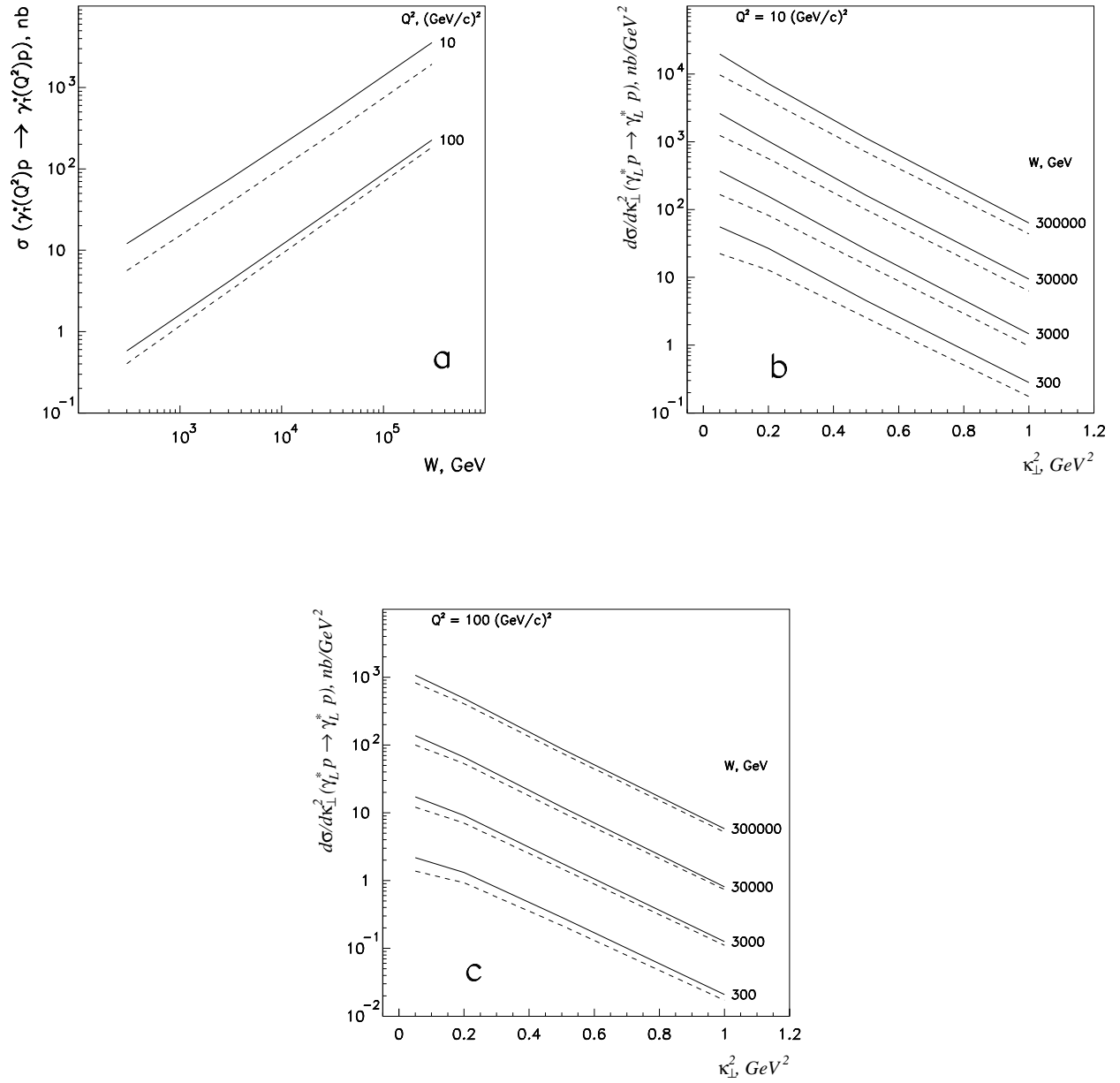


FIG. 6. The same as in Fig. 4 for reaction $\gamma_T^*(Q^2)p \rightarrow \gamma_T^*(Q^2)p$.

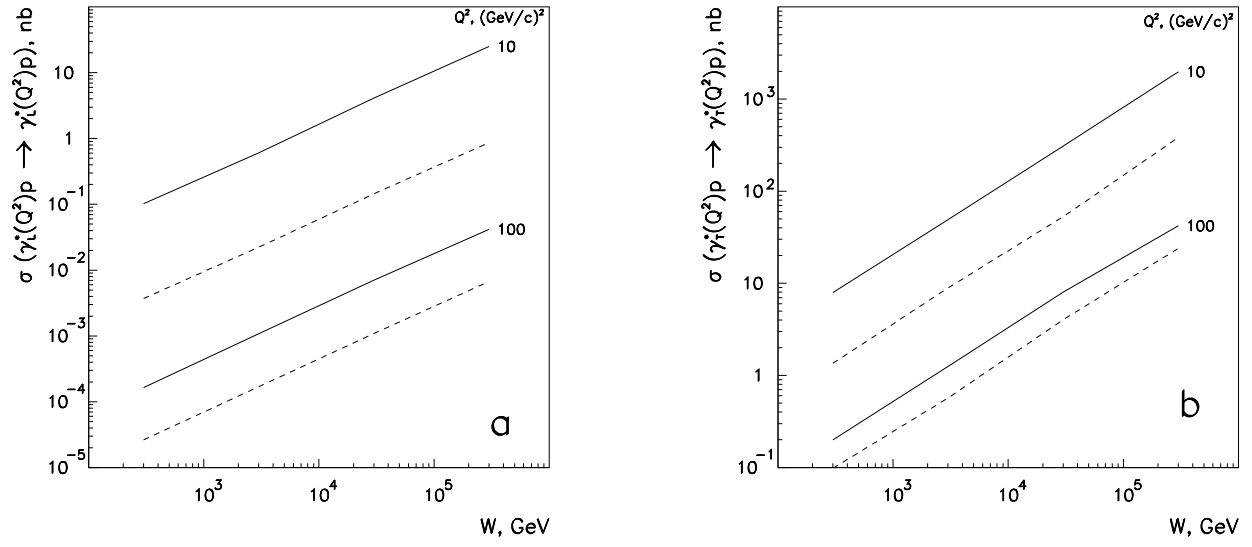


FIG. 7. Cross sections $\gamma_{L,T}^*(Q^2)p \rightarrow \gamma_{L,T}^*(Q^2)p$ with scale factor $W^2/(M_{q\bar{q}}^2 + M_{q\bar{q}'}^2)$.

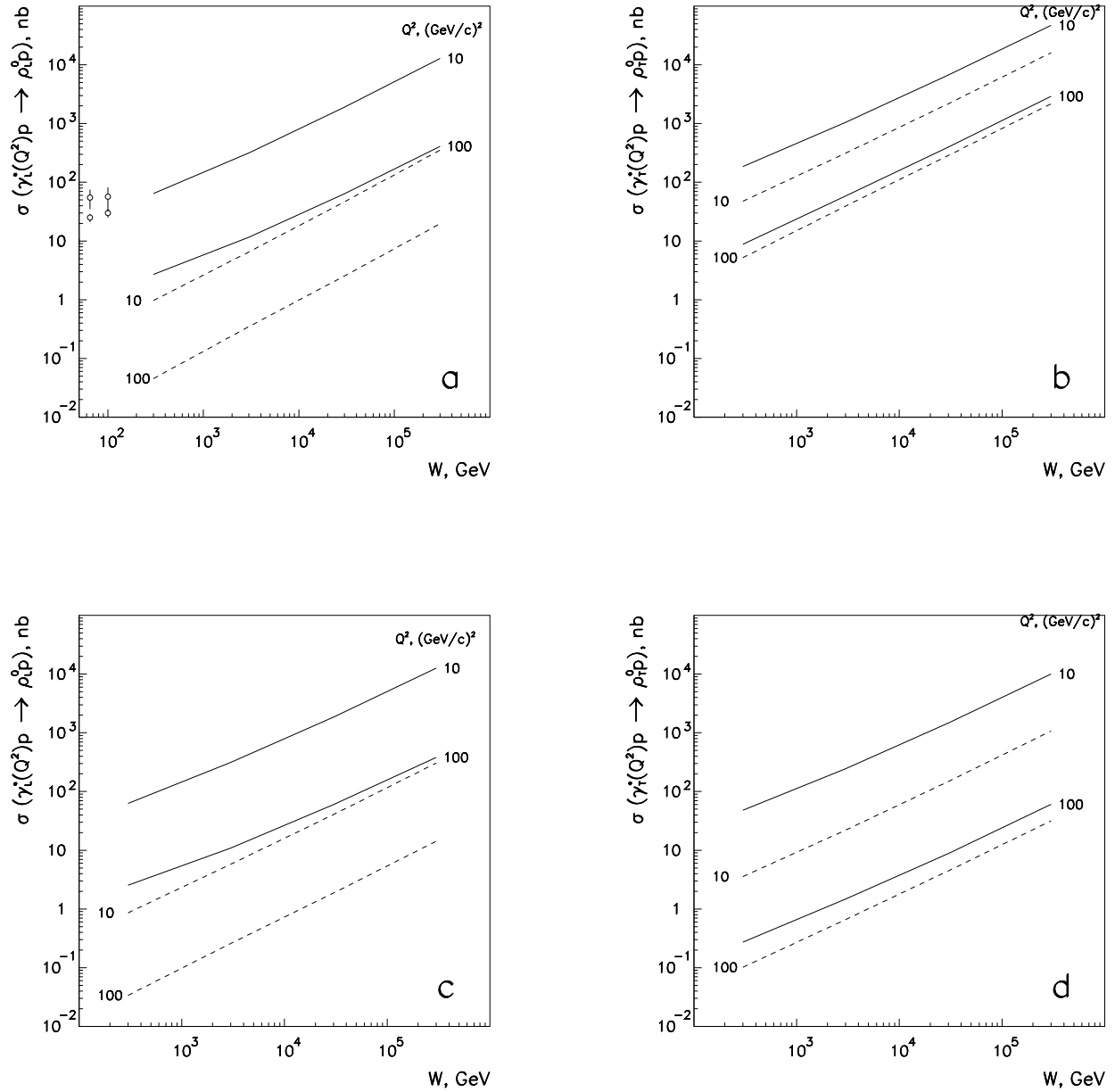


FIG. 8. Cross sections in reactions $\gamma_{L,T}^*(Q^2)p \rightarrow \rho_{L,T}^0$ with scale factor $W^2/(Q^2 + \mu_V^2)$. a,b Variant $G_\rho(M_{q\bar{q}}^{\prime 2}) \sim \text{const}$ at large $M_{q\bar{q}}^{\prime 2}$; c,d $G_\rho(M_{q\bar{q}}^{\prime 2}) \sim 1/M_{q\bar{q}}^{\prime 2}$ at large $M_{q\bar{q}}^{\prime 2}$. Experimental data shown in Fig. 8a are taken from [18]; they are used for fixing the constant C in Eq. (49).